54
Review paper
Doi 10.7251/stp2024401028S
ISSN 2566-4484

Nikola Santrač, University of Novi Sad, nikola.santrac@polj.uns.ac.rs
Mehmed Batilović, University of Novi Sad, mehmed@uns.ac.rs
Marko Marković, University of Novi Sad, marko_m@uns.ac.rs
Miro Govedarica, University of Novi Sad, miro@uns.ac.rs
Pavel Benka, University of Novi Sad, pavel.benka@polj.uns.ac.rs

APPLICATION OF CLOSE-RANGE UAV PHOTOGRAMMETRY IN THE DETECTION OF CRACKS ON FACADE

Abstract

The photogrammetric survey of buildings is a beneficial process to obtain accurate 3D data for facade inspection. It allows more straightforward monitoring of the state of the facade over time. An orthomosaic with an average ground sampling distance of 2.1 mm is created using close-range unmanned aerial vehicle photogrammetry. Ground control points, determined with millimeter accuracy from the geodetic network, were used for georeferencing. Resulting in an average ground control points residual of 1.6 mm. Based on the created orthomosaic, visual detection of cracks in the facade was performed. Also, an orthomosaic created with this accuracy can be a basis for automatic tools for detecting cracks on the facade.

Keywords: building facade, UAV technology, image processing, crack detection

ПРИМЕНА БЛИСКОПРЕДМЕТНЕ УАВ ФОТОГРАМЕТРИЈЕ У ДЕТЕКЦИЈИ ПУКОТИНА НА ФАСАДАМА

Сажетак

Фотограметријски премјер објеката је користан поступак за креирање 3Д модела у сврху инспекције фасаде. Омогућава једноставније праћење стања фасаде током времена. Ортомозаик, са величином пиксела у природи од 2.1 mm, је креиран примјеном блископредметне УАВ фотограметрије. Контролне тачке, одређене са милиметарском тачношћу са геодетске мреже, су коришћене за георефернцирање. То је утицало на веома малу грешку дефинисања контролних тачака која износи 1.6 mm. На основу креираног ортомозаика извршена је визуелна детекција пукотина на фасади. Ортомозаик креиран са наведеном тачношћу може послужити као подлога алатима за аутоматску детекцију пукотина на фасади.

Кључне ријечи: фасада, беспилотна летелица, обрада фотографија, детекција пукотина

1. INTRODUCTION

Monitoring and maintaining structures such as buildings and bridges is a crucial but expensive job to ensure safe operation. Traditional monitoring methods involve regular visual inspections, often requiring inspectors to assess the level of deterioration. Automating this process can significantly reduce cost and time between inspections [1]. An essential task of this inspection is to represent a building's facade, which is exposed to external environmental conditions. The crack on the facade poses is the first of the signs of the deterioration of the building, which underlines the need for regular inspections and maintenance. It is important to ensure that the facade elements and all external installations attached to the facade remain intact. Early detection of cracks can help to prevent the potential collapse of the facade and building. However, given the increasing height of buildings and the growing complexity of facade elements, inspecting a building facade is often challenging [2].

3D modeling created based on images captured by high-resolution cameras on unmanned aerial vehicles (UAVs) is becoming a popular and cost-effective alternative [3]. Recent advances in sensors and flight systems have expanded the use of UAVs in various fields, such as forestry [4], agriculture [5], surveying [6], construction [7], facade inspection [8], and various other fields. Reducing labor, time, and cost resources has enabled more frequent facade inspections [9]. When assessing the condition of the facade, the close-up images taken by the UAV are currently obtained by manual adjustment [10], and cracks in each image are identified. However, this often neglects the integration of building model information, which hinders the localization and documentation of detected facade anomalies. There is a need to integrate and manage large amounts of spatio-temporal image data from different sources to improve their accessibility and usability for automated facade inspection.

The Structure from Motion (SfM) algorithm was developed to reconstruct a surface or object by aligning tie points obtained from multiple images, where each point contains both position and color information extracted from an image [11]. The SfM algorithm produces a sparse point cloud, and the Multi-View Stereo (MVS) algorithm generates a dense point cloud. In the SfM-MVS workflow, there are two approaches to georeferencing the images. The first is direct georeferencing, which uses navigation sensors integrated into UAVs, mainly Global Navigation Satellite Systems (GNSS) [12], and the second is indirect georeferencing, which uses Ground Control Points (GCPs). In most studies, the coordinates of the GCPs are determined using GNSS rovers with the Real-Time Kinematic (RTK) method. The accuracy of the coordinate determination depends on the model and manufacturer of the instrument. Nevertheless, it can be said that the coordinates are determined with a horizontal and vertical accuracy of < 10 mm and < 15 mm, respectively [13].

Improving the accuracy of GCPs can be achieved by stabilizing a geodetic network. The accuracy within a geodetic network depends on various factors, e.g., the shape and size of the network, measurement method, used instrument, number of GCPs and measurements, degrees of freedom, and more. Accurately determining coordinates within a geodetic network can be several millimeters [14]. This approach eliminates errors that may have occurred when determining the GCPs. The standard 3D accuracy with which the GCPs are determined in software processing is given as 20 mm [15] and 5 mm [16], however, are they determined with that accuracy. The final products of UAV photogrammetry include orthomosaic, Digital Elevation Model (DEM), 3D models, or mesh and point clouds. The accuracy of orthomosaic and DEM can be expressed by the Ground Sampling Distance (GSD), which represents the distance between the centers of adjacent pixels on the ground and is calculated based on the flight altitude, distance from the terrain or object, and camera specifications (image width, sensor width, and focal length). Proper acquisition and sensor calibration should result in a model with a relative accuracy within 1-3 times the GSD value. However, the absolute accuracy of the model is somewhat lower, typically between 1-2 times the GSD value in the east and north axes and 1-3 times in the vertical axis [17].

In this paper, images of the object were taken using UAV and then processed with software that uses the SfM algorithm. Georeferencing was conducted using GCPs located on the object facade with millimeter accuracy. This accuracy was achieved using a geodetic network, appropriate instruments, and measurement methods. The final processing results consist of an orthomosaic on which cracks were detected.

2. MATERIAL AND METHODS

The procedure used in this paper is given in Figure 1. Each of the steps is explained in the following chapters.

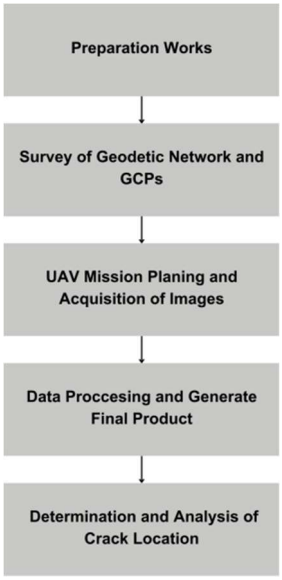

Figure 1. Workflow

2.2. OBJECT INSPECTION

The UAV dataset was acquired in the urban area of Novi Sad, Serbia, approximately 45°14' 27" N and 19° 50' 17" E. The case study focused on the northwest facade of a high-rise (13-storey) residential building built in 1972. The location of the study area and building is depicted in Figure 2. From the first to the 13th floor, the northern facade of the building is identical in appearance, with windows on the left and right edges of the building and a terrace in the middle of each floor. While on the ground floor in the middle of the building, there is an abandoned transformer station.

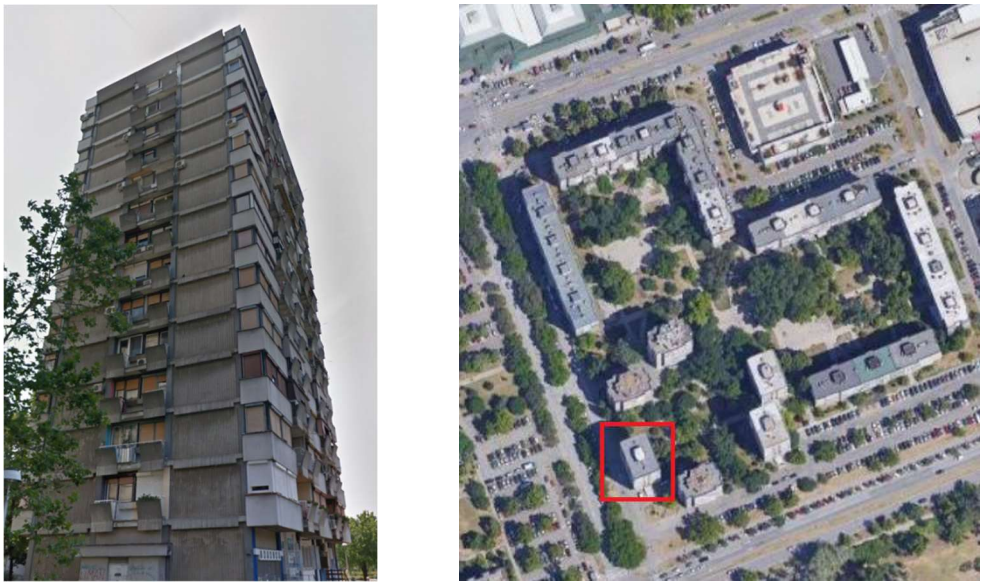

a) *b)*

Figure 2. a) Northwest facade of the object (from Google Maps-Street View©) b) location of the object in urban building block (from Google Maps©)

2.3. ESTABLISHMENT OF GEODETIC NETWORK AND GCPS

To determine the GCPs coordinates with millimeter accuracy, the geodetic network with 3 points (1–3) and 13 GCPs on the facade (46–58) is stabilized, as depicted in Figure 3a and Figure 3b. The GCPs on the facade represented existing characteristic details such as screws, point damage, or corner of a concrete block. The measurements were conducted on the same day as the UAV survey to obtain reliable information about the observations. A total of n=96 observations were performed (32 horizontal directions, 32 zenith angles, and 32 slope distances). Measurements between the points of the geodetic network were executed using one repetition in both faces of the instrument and prism as reflectors. All GCPs on the object were measured from point 3 in two repetitions on both faces of the instrument with non-prism mode. Observations of horizontal directions, slope distances, and zenith angles were carried out using the *Trimble S5* robotic total station with standard deviations σ_α=2″, σ_d=1 mm + 2 ppm prism and σ_d=2 mm + 2 ppm non-prism, and σ_Z= 2″ [18]. The number of unknown parameters was u=51 (48 unknown coordinates and three unknown orientations), with a defect datum of the geodetic network de=4. The degrees of freedom (f=n−u+de) amounted to 49. Approximate coordinates of geodetic network points were determined using the GNSS RTK method in the MGI / 1901 Balkans zone 7 coordinate system (EPSG: 3909). The Gauss-Markov adjustment model with the least squares method is used to adjust the geodetic network. This model constitutes a linear or linearized mathematical model dealing with functional and stochastic components, defining relationships between stochastically realized observations and unknown parameters of geodetic networks. The datum is defined with a minimal trace on all geodetic network points (1-3). The coordinates and standard deviations of all points are given in Table 1. Table 2 shows the measures of central tendency and dispersions of geodetic network points and GCPs standard deviation.

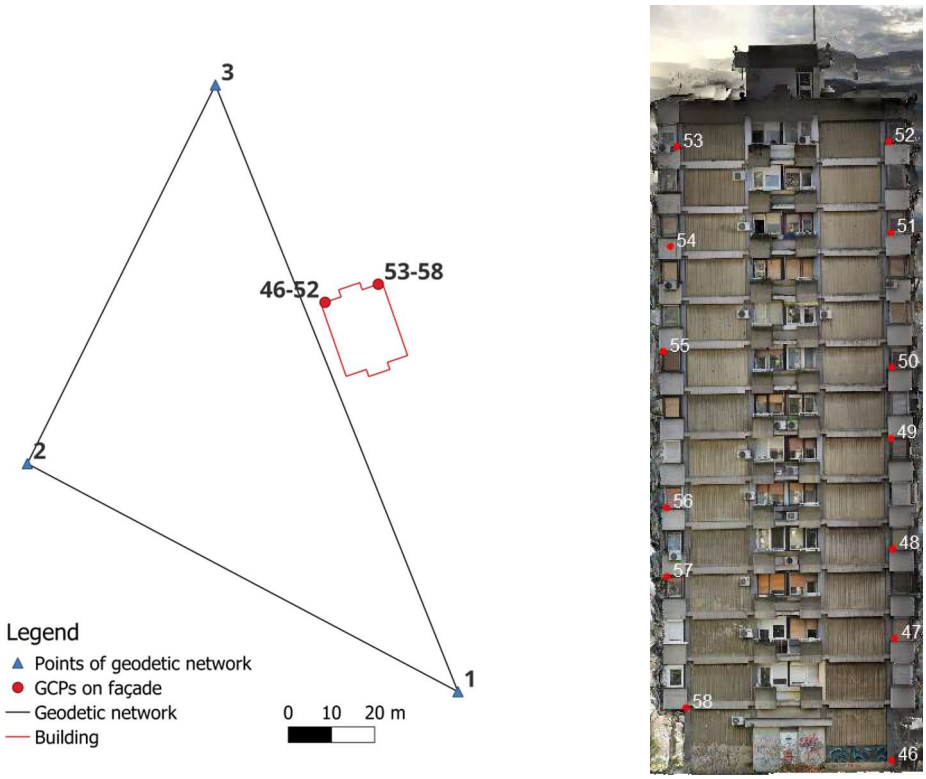

a) *b)*

Figure 3. a) Geodetic network and b) location of GCPs on the facade

Table 2. Coordinates and standard deviation of geodetic network points and GCPs

Point	E [m]	N [m]	H [m]	σ_E [mm]	σ_N [mm]	σ_H [mm]	σ_{3D} [mm]
1	7409223.727	5011282.613	84.603	0.3	0.4	0.4	0.6
2	7409124.065	5011335.415	84.945	0.3	0.4	0.3	0.6
3	7409167.596	5011423.089	85.830	0.2	0.4	0.3	0.6
46	7409192.741	5011372.688	86.206	0.6	1.0	0.4	1.2
47	7409192.562	5011372.724	93.793	0.6	1.0	0.4	1.2
48	7409192.520	5011372.741	99.393	0.6	1.0	0.5	1.2
49	7409192.630	5011372.712	106.251	0.6	1.0	0.5	1.2
50	7409192.531	5011372.722	110.662	0.5	0.9	0.6	1.2
51	7409192.432	5011372.900	116.173	0.5	0.9	0.6	1.2
52	7409192.524	5011372.711	124.673	0.5	0.9	0.7	1.2
53	7409205.132	5011376.552	124.747	0.6	0.8	0.7	1.2
54	7409205.621	5011376.858	118.361	0.7	0.9	0.6	1.2
55	7409205.931	5011376.913	111.896	0.7	0.9	0.6	1.2
56	7409205.953	5011376.844	102.206	0.7	0.9	0.5	1.2
57	7409205.982	5011376.826	97.791	0.7	0.9	0.5	1.2
58	7409204.957	5011376.680	89.750	0.7	0.9	0.4	1.2

Table 1. Central tendency and dispersions of geodetic network points and GCPs standard deviation

	Points of the geodetic network (1-3)				GCP (46-58)			
	σ_E [mm]	σ_N [mm]	σ_H [mm]	σ_{3D} [mm]	σ_E [mm]	σ_N [mm]	σ_H [mm]	σ_{3D} [mm]
Min.	0.2	0.4	0.3	0.6	0.5	0.8	0.4	1.2
Max.	0.3	0.4	0.4	0.6	0.7	1.0	0.7	1.2
Average	0.3	0.4	0.3	0.6	0.6	0.9	0.5	1.2
Median	0.3	0.4	0.3	0.6	0.6	0.9	0.5	1.2
Range	0.1	0.1	0.1	0.0	0.2	0.2	0.3	0.0
Standard deviation	0.1	0.0	0.1	0.0	0.1	0.1	0.1	0.0

2.4. UAV MISSION PLANNING AND ACQUISITION OF IMAGES

Parrot ANAFI UAV is used for collecting images, and the technical specifications are shown in Table 3. The UAV is an integrated GNSS receiver supporting both GPS and GLONASS satellites. However, UAVs with a standard GNSS receiver provide image geolocation with an expected accuracy of a few meters [19], and in urban areas, the signal is often interrupted by the buildings [20]. The coordinates are stored in the EXIF file attached to each image, expediting the processing as the software searches for tie points only in overlapping photographs relatively close to each other. Considering the acquisition process and potential challenges posed by external elements such as terraces, power cables, and trees obstructing the facade, a manual flight mode was chosen. The flight mission involved executing flights with the camera positioned perpendicular to the facade at an approximate distance of 6 meters. Taking into the equation the distance from the facade and the technical specifications of the UAV camera, the GSD for the UAV images was calculated to be 2.1 mm. The survey's flight mission involved selecting vertical flying strips. Image overlap is 86% vertical and 89% horizontal, and 492 images were collected.

Table 2. Technical specifications of the Parrot ANAFI UAV [21]

UAV Specifications	
Size unfolded	240 × 175 × 65 mm
Weight	320 g
Max. flight time	25 min
Operating temperature range	−10 ◦C to 40 ◦C
Max. horizontal speed	15 m/s
Max. vertical speed	4 m/s
Max. transmission range	4 km with controller
Max. wind resistance	50 km/h
Satellite Positioning Systems	GPS & GLONASS
Camera Specifications	
Sensor format	6.194 × 4.646 mm
Sensor	1/2.4” CMOS
Lens	FOV 180◦
ISO range	100–3200
Image resolution	4608 × 3456 px
Focal length	4 mm
Diagonal crop	factor 7.487

2.5. DATA PROCESSING AND GENERATING ORTHOMOSAIC

After the images were collected, the Agisoft Metashape software package began processing data. The Root Mean Square Error (RMSE) reproject error using the camera optimization feature is enhanced. This process followed the methodology explained in [22], with the computation parameters listed in Table 4. Through this procedure, low-quality tie points were systematically eliminated from the sparse point cloud after the alignment of images. The reconstruction uncertainty metric identified points exhibiting poor geometric relations between cameras. Tie points with inadequate match accuracies were singled out using the projection accuracy criterion. Additionally, tie points resulting from false matches were identified and removed based on the reprojection error criterion. These selection and elimination processes were conducted iteratively. The removal of poor tie points aimed to improve the estimated internal and external orientation parameters. However, each iteration of tie point removal altered the accuracies of the remaining tie points, necessitating reoptimization of the project before proceeding.

Table 3. Computing parameters of the software

Alignment	
Accuracy	High
Generic preselection	Enable
Reference preselection	Source
Key point limit	60 000
Tie point limit	0 (unlimited)
Dense cloud building	
Quality	High
Depth filtering	Mild

For georeferencing, GCPs obtained with an average accuracy of 1.2 mm (Table 2) were used, and that accuracy is entered into the software during GCPs input. Table 5 shows the residuals for GCPs in processing, their measures of central tendency, dispersions, and RMSE.

The process results in a georeferenced point cloud with 116 million points (Figure 4a). The created point cloud generates the orthomosaic with an average GSD of 2.1 mm (Figure 4b). The achieved average GSD of the generated orthomosaic corresponds to the GSD of the initial images, determined in the flight planning phase. Analysis of orthomosaic shows that most of the details on the facade

are realistically presented. Thanks to well-planned data collection, this also applies to the edges of the facade surface, even though fewer images are overlapped in these zones than in the central parts.

Table 4. GCPs residuals

Point	E [mm]	N [mm]	H [mm]	3D [mm]
46	0.1	-1.0	1.4	1.7
47	-0.1	0.1	-0.7	0.7
48	-2.1	-1.0	-1.3	2.6
49	-0.8	1.0	0.7	1.5
50	2.0	0.9	-2.9	3.6
51	0.8	-0.9	1.9	2.2
52	0.0	0.6	1.5	1.6
53	-0.2	0.0	0.0	0.2
54	-1.3	-0.5	-0.4	1.4
55	-0.5	-0.4	0.0	0.7
56	0.5	0.4	0.1	0.7
57	1.2	-0.6	1.0	1.7
58	0.6	1.3	-0.7	1.6
Min.	-2.1	-1.0	-2.9	0.2
Max.	2.0	1.3	1.9	3.6
Average	0.0	0.0	0.0	1.6
Median	0.0	0.0	0.0	1.6
Range	4.0	2.3	4.7	3.4
Standard deviation	1.1	0.8	1.3	1.4
RMSE	1.0	0.8	1.2	1.8

a) *b)*

Figure 4. a) point cloud and b) orthomosaic of the facade

3. DISCUSSIONS

During the analysis of the orthomosaic, cracks found on the facade are shown in Figure 5. It can be concluded that the cracks appeared on different parts of the facade. However, the procedure of manual detection of cracks on the orthomosaic is time consuming and laborious. The detection and classification of cracks largely depend on the individual expertise and experience of the surveyor and lead to data redundancy. In addition to the manual analysis of cracks on the facade, there are tools for automatically detecting cracks on the orthomosaic facade, such as the AIM method [23]. After detecting cracks on the georeferenced orthomosaic, it is possible to determine the coordinates of those cracks on the object in the global coordinate system, in this case, EPSG: 3909. Since a geodetic network and GCPs with an accuracy of several mm have been established, it is possible to mark the cracks on the object with very high precision.

a) *b)*

c) *d)*

Figure 5. Cracks on the facade

4. CONCLUSION

This paper presents the procedure for detecting cracks on the facade of a 13-story building. Cracks were detected on an orthomosaic created using a SfM algorithm based on images collected from a UAV. GCPs measured from an established geodetic network were used for georeferencing. The average standard deviation of GCP determination is 1.2 mm, while the average accuracy of georeferencing (GCP residuals) was 1.6 mm. This accuracy makes it possible to detect even the most minor cracks in the facade, and the minimum number of pixels that can detect a target is at least a 2-pixel square (2x2 pixel), even for high-contrast images. In some conditions might need to consider a 4-pixel square [24].

Along with manual detection of cracks on the facade, there is also an automatic one. However, the efficiency, reliability, accuracy, and objectivity of the automated building facade inspection process depend on the ability of the applied model to identify, locate, and quantify damage on images acquired by the UAV. One of the reasons for the appearance of cracks on this building is that residential buildings built with industrial building technology in Novi Sad in the second half of the XX century indicated the unsatisfactory technical condition of facade elements [25].

ACKNOWLEDGEMENT

This research has been supported by the Ministry of Science, Technological Development and Innovation (Contract No. 451-03-65/2024-03/200156) and the Faculty of Technical Sciences, University of Novi Sad through project "Scientific and Artistic Research Work of Researchers in Teaching and Associate Positions at the Faculty of Technical Sciences, University of Novi Sad" (No. 01-3394/1).

LITERATURE

[1] I. Abdel-Qader, O. Abudayyeh, and M. E. Kelly, "Analysis of edge-detection techniques for crack identification in Bridges," Journal of Computing in Civil Engineering, vol. 17, no. 4, pp. 255–263, Oct. 2003. doi:10.1061/(asce)0887-3801(2003)17:4(255)

[2] Y. Liu, J. K. Yeoh, and D. K. Chua, "Deep learning–based enhancement of motion blurred UAV concrete crack images," *Journal of Computing in Civil Engineering*, vol. 34, no. 5, 2020. doi:10.1061/(asce)cp.1943-5487.0000907

[3] M. W. Smith, J. L. Carrivick, and D. J. Quincey, "Structure from motion photogrammetry in physical geography," *Progress in Physical Geography: Earth and Environment*, vol. 40, no. 2, pp. 247–275, Nov. 2015. doi:10.1177/0309133315615805

[4] N. Kranjec, M. Triglav Čekada, and M. Kobal, "Predicting tree species based on the geometry and intensity of Aerial Laser Scanning Point Cloud of Treetops," *Geodetski vestnik*, vol. 65, no. 02, pp. 234–259, 2021. doi:10.15292/geodetski-vestnik.2021.02.234-259

[5] J. Su, X. Zhu, S. Li, and W.-H. Chen, "AI meets uavs: A survey on AI empowered UAV Perception Systems for Precision Agriculture," *Neurocomputing*, vol. 518, pp. 242–270, Jan. 2023. doi:10.1016/j.neucom.2022.11.020

[6] [5] H. Sertić, R. Paar, H. Tomić, and F. Ravlić, "Influence of flight height and image sensor on the quality of the UAS orthophotos for cadastral survey purposes," *Land*, vol. 11, no. 8, p. 1250, Aug. 2022. doi:10.3390/land11081250

[7] W. W. Greenwood, J. P. Lynch, and D. Zekkos, "Applications of uavs in Civil Infrastructure," *Journal of Infrastructure Systems*, vol. 25, no. 2, Jun. 2019. doi:10.1061/(asce)is.1943-555x.0000464

[8] C. Eschmann and T. Wundsam, "Web-based georeferenced 3D inspection and monitoring of bridges with Unmanned Aircraft Systems," *Journal of Surveying Engineering*, vol. 143, no. 3, Aug. 2017. doi:10.1061/(asce)su.1943-5428.0000221

[9] J. Seo, L. Duque, and J. Wacker, "Drone-enabled bridge inspection methodology and application," *Automation in Construction*, vol. 94, pp. 112–126, Oct. 2018. doi:10.1016/j.autcon.2018.06.006

[10] D. Mader, R. Blaskow, P. Westfeld, and C. Weller, "Potential of UAV-based laser scanner and multispectral camera data in building inspection," *The International Archives of the Photogrammetry, Remote Sensing and Spatial Information Sciences*, vol. XLI-B1, pp. 1135–1142, Jun. 2016. doi:10.5194/isprs-archives-xli-b1-1135-2016

[11] M. J. Westoby, J. Brasington, N. F. Glasser, M. J. Hambrey, and J. M. Reynolds, "'structure-from-motion' photogrammetry: A low-cost, effective tool for Geoscience Applications," *Geomorphology*, vol. 179, pp. 300–314, Dec. 2012. doi:10.1016/j.geomorph.2012.08.021

[12] T. Türk, N. Tunalioglu, B. Erdogan, T. Ocalan, and M. Gurturk, "Accuracy assessment of UAV-post-processing Kinematic (PPK) and UAV-traditional (with ground control points) georeferencing methods," *Environmental Monitoring and Assessment*, vol. 194, no. 7, Jun. 2022. doi:10.1007/s10661-022-10170-0

[13] P. Martínez-Carricondo, F. Agüera-Vega, and F. Carvajal-Ramírez, "Accuracy assessment of RTK/PPK UAV-photogrammetry projects using differential corrections from multiple GNSS fixed base stations," *Geocarto International*, vol. 38, no. 1, Apr. 2023. doi:10.1080/10106049.2023.2197507

[14] D. Janos and P. Kuras, "Evaluation of low-cost GNSS receiver under demanding conditions in RTK Network mode," *Sensors*, vol. 21, no. 16, p. 5552, Aug. 2021. doi:10.3390/s21165552

[15] Pix4dMapper Support, User Manual, https://support.pix4d.com/hc/en-us/sections/360003718992-Manual (accessed Jan. 26, 2024).

[16] Agisoft Metashape Professional Edition, version 2.0 User Manuals, https://www.agisoft.com/pdf/metashape-pro_2_0_en.pdf (accessed Jan. 26, 2024).

[17] E. Sanz-Ablanedo, J. Chandler, J. Rodríguez-Pérez, and C. Ordóñez, "Accuracy of Unmanned Aerial Vehicle (UAV) and SFM photogrammetry survey as a function of the number and

location of ground control points used," *Remote Sensing*, vol. 10, no. 10, p. 1606, Oct. 2018. doi:10.3390/rs10101606

[18] "Trimble S5: Total stations," Trimble S5 | Total Stations | Trimble Geospatial, https://geospatial.trimble.com/en/products/hardware/trimble-s5 (accessed Jan. 26, 2024).

[19] What is the relative and absolute accuracy of drone mapping, https://support.pix4d.com/hc/en-us/articles/202558889-What-is-the-relative-and-absolute-accuracy-of-drone-mapping (accessed Jan. 26, 2024).

[20] J. Choi, C. Yeum, S. Dyke, and M. Jahanshahi, "Computer-aided approach for rapid post-event visual evaluation of a building facade," *Sensors*, vol. 18, no. 9, p. 3017, Sep. 2018. doi:10.3390/s18093017

[21] "Parrot Anafi work drone - technical specifications," Parrot, https://www.parrot.com/en/drones/technical-specifications-anafi-work (accessed Jan. 26, 2024).

[22] S. Draganić *et al.*, "Orthofacade-based assisted inspection method for buildings," *Applied Sciences*, vol. 12, no. 11, p. 5626, Jun. 2022. doi:10.3390/app12115626

[23] [4] J.-S. R. Over *et al.*, "Processing coastal imagery with Agisoft metashape professional edition, version 1.6—structure from Motion Workflow Documentation," *Open-File Report*, 2021. doi:10.3133/ofr20211039

[24] "Concept of minimum detectable object size: Machine Vision Basics: Keyence America," KEYENCE, https://www.keyence.com/ss/products/vision/visionbasics/basic/practice02/#:~:text=Although%20the%20minimum%20size%20from,square%20depending%20on%20the%20conditions (accessed Jan. 26, 2024).

[25] M. Laban, "The Improvement of Envelopes' Performances of Multi-Storey Prefabricated and Semi-Prefabricated Residential Buildings in Novi Sad," thesis, 2012